AGU ADVANCING EARTH AND SPACE SCIENCE

Geophysical Research Letters

RESEARCH LETTER
10.1029/2020GL089765

Measurements of Iceberg Melt Rates Using High-Resolution GPS and Iceberg Surface Scans

Kristin M. Schild[1,2,3], David A. Sutherland[1], Pedro Elosegui[4,5], and Daniel Duncan[6]

[1]Department of Earth Sciences, University of Oregon, Eugene, OR, USA, [2]Now at School of Earth and Climate Sciences, University of Maine, Orono, ME, USA, [3]Now at Climate Change Institute, University of Maine, Orono, ME, USA, [4]Massachusetts Institute of Technology, Westford, MA, USA, [5]Institute of Marine Sciences, ICM-CSIC, Barcelona, Spain, [6]Institute of Geophysics, University of Texas, Austin, TX, USA

Abstract Increasing freshwater input to the subpolar North Atlantic through iceberg melting can influence fjord-scale to basin-scale ocean circulation. However, the magnitude, timing, and distribution of this freshwater have been challenging to quantify due to minimal direct observations of subsurface iceberg geometry and melt rates. Here we present novel in situ methods capturing iceberg change at high-temporal and -spatial resolution using four high-precision GPS units deployed on two large icebergs (>500 m length). In combination with measurements of surface and subsurface geometry, we calculate iceberg melt rates between 0.10 and 0.27 m/d over the 9-day survey. These melt rates are lower than those proposed in previous studies, likely due to using individual subsurface iceberg geometries in calculations. In combining these new measurements of iceberg geometry and melt rate with the broad spatial coverage of remote sensing, we can better predict the impact of increasing freshwater injection from the Greenland Ice Sheet.

Plain Language Summary The acceleration of Greenland glaciers has led to an increase of icebergs discharged in nearby waters. As icebergs melt, they release freshwater into salty ocean waters, impacting local circulation. In order to understand how global circulation will change in the future, we need accurate iceberg melt rates. To do this, we use measurements of mass loss from on-iceberg GPS units, and three-dimensional iceberg geometry constructed from aerial drone and subsurface sonar data. We found melt rates smaller than previous studies and strong evidence for variable overall melt rates with different keel depths and over time. This study is the first of its kind to calculate melt rates using exact iceberg geometry. To better predict iceberg impacts, future iceberg studies should take these geometry results into account.

Key Points:

- High resolution on-iceberg GPS units show temporally variable melt rate over the 9-day survey period
- Contrasting melt rates between different sized icebergs supports the hypothesis of depth-variable melt rates
- Melt rates are lower than prior studies, likely due to using observed subsurface geometry (not idealized or end-member) in calculations

Supporting Information:

- Supporting Information S1

Correspondence to:
K. M. Schild,
kristin.schild@maine.edu

Citation:
Schild, K. M., Sutherland, D. A., Elosegui, P., & Duncan, D. (2021). Measurements of iceberg melt rates using high-resolution GPS and iceberg surface scans. *Geophysical Research Letters*, *48*, e2020GL089765. https://doi.org/10.1029/2020GL089765

Received 10 JUL 2020
Accepted 18 NOV 2020

1. Introduction

The six-fold increase in mass loss from Greenland since the 1980s (Mouginot et al., 2019) has increased the number of icebergs choking Greenlandic fjords. The melting and transit of these icebergs has the potential to modify ocean currents (Allan & Allan, 2019; Bamber et al., 2012; Good et al., 2018; Marsh et al., 2010; Yang et al., 2016), freshen the North Atlantic, influence Arctic and subarctic climates (e.g., Dukhovskoy et al., 2019), and become hazardous to ship-based travel (Gagnon & Wang, 2012) and offshore installations (e.g., McKenna, 2005). However, the prolonged impact of increasing icebergs on local and regional ocean circulation remains unclear, largely due to uncertainties concerning iceberg melt rate, meltwater distribution with depth, and iceberg residence time.

Early studies on iceberg melt used a combination of laboratory experiments (Josberger, 1978), field observations (El-Tahan et al., 1987; Venkatesh et al., 1985), and empirical relationships (Weeks & Campbell, 1973; White et al., 1980) to calculate freshwater loss. More recent studies have refined these equations, uncertainties, and dominant deterioration processes (e.g., A. J. Crawford, Mueller, & Joyal, 2018; FitzMaurice et al., 2018), and incorporated remote sensing (Enderlin et al., 2016, 2018; Enderlin & Hamilton, 2014; Sulak et al., 2017), modeling (e.g., Moon et al., 2018) and in situ measurements into melt calculations. Remote sensing expanded the reach of laboratory measurements; however, satellite remote sensing is limited by spatial and temporal resolution and cannot yet image subsurface iceberg geometry, therefore these studies assumed an idealized subsurface geometry (e.g., cone, cylinder) to calculate melt rate (m/d), which resulted

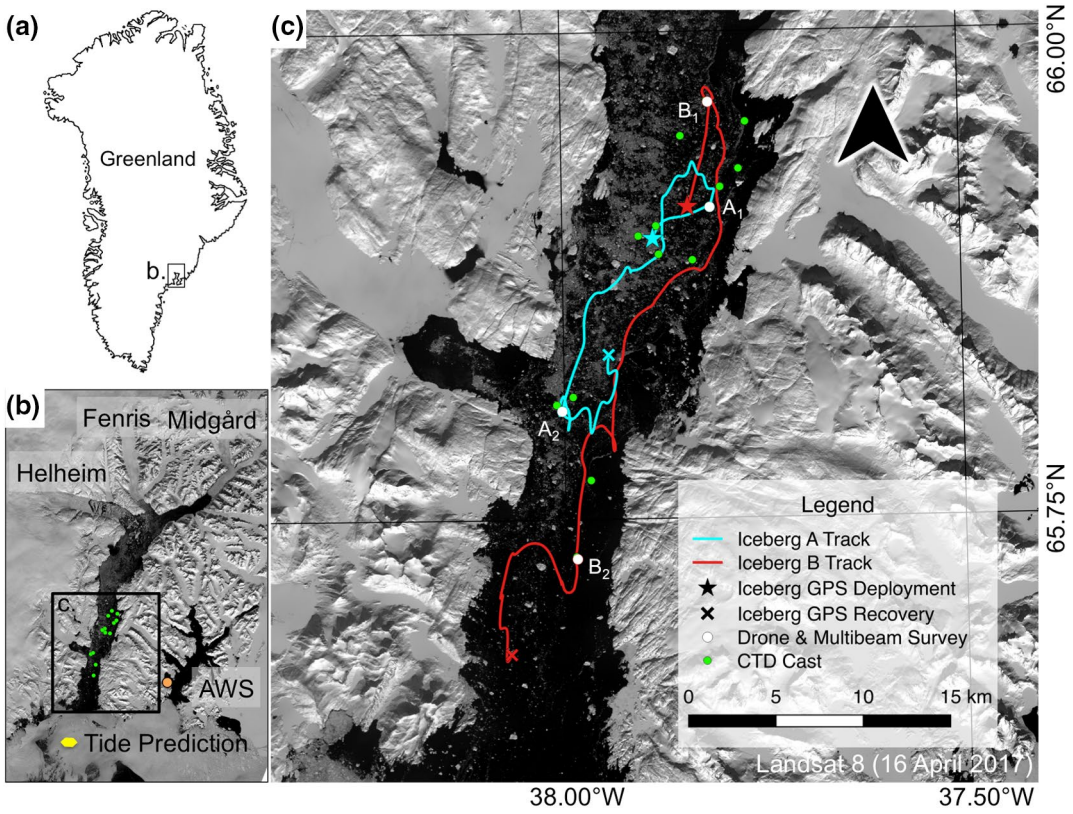

Figure 1. Sermilik Fjord, southeast Greenland (a, b), with Iceberg A (c, cyan line) and B (c, red line) tracks from 15 to 24 July 2017. The locations of the drone and multibeam iceberg surveys (c, white labeled circles) on July 16, 2017 (A_1, B_1) and July 21, 2017 (A_2, B_2), CTD casts (b, c, green circles), and the locations used for the tidal correction (b, yellow hexagon) and atmospheric pressure correction (b, orange circle, AWS) are noted.

in large uncertainties (8%–100%; Enderlin & Hamilton, 2014). Modeling studies (e.g., Moon et al., 2018) have isolated individual melt mechanisms by applying theoretical parameterizations to generalized iceberg geometries. However, this generalized iceberg geometry mimics icebergs far from their source glacier (Barker et al., 2004), at which point the icebergs have deteriorated to more stable geometries (Wagner et al., 2017). In this study, we instrument icebergs in Sermilik Fjord, the largest fjord system in southeast Greenland, with high-precision GPS to directly measure surface lowering. We use coincident ship-based drone and multibeam sonar data to construct full-iceberg geometries, then derive volume flux and melt rates based upon measured surface lowering and iceberg geometry. By using individual iceberg geometry to calculate volume loss, we avoid generic or idealized subsurface shapes, and derive iceberg melt rates at temporal and spatial resolutions well beyond previous studies (every 5–30 s, ≤ ±1.3 mm).

2. Methods

2.1. On-Iceberg GPS

To enable coincident on-iceberg and ship-based measurements, we selected icebergs that were accessible by boat (lower iceberg distribution), located in the mid-fjord region (stays in the fjord during surveying; Figure 1), appeared stable enough to remain upright for the duration of our campaign (equipment recovery), and large enough for helicopter GPS deployment and recovery (>500 m length). We deployed four high-spatial (≤±3 cm) and high-temporal (5–30 s) resolution geodetic GPS units (measuring three-dimensional positions, *lat-lon-h*) in tandem on two icebergs using a Bell 212 helicopter. Tandem GPS configuration enables measurements of iceberg rotation, deterioration, and tipping. To locate the instrumented icebergs during ship-based surveying, we also deployed expendable GPS units (Globalstar SmartOne C, two-dimensional

positions, *lat-lon*) adjacent to each high-resolution unit, relaying the position to an online server every hour (similar to Sutherland, Roth, et al., 2014).

The geodetic GPS units recorded the absolute height of each iceberg, therefore, we removed the tidal phase (<3.3 m), atmospheric pressure (inverse barometer, <0.3 m), and variations in the geoid—ellipsoid offset (changes in relative sea level, <0.65 m) along the iceberg tracks to isolate surface lowering due solely to ablation (see Supporting Information Text S1 for expanded methods). Lastly, we removed signal interference caused by the adjacent (uncertainties ≥ 0.5 m) and across-iceberg (one standard deviation) expendable GPS devices, and applied a 40-h Hanning filter to remove the remaining high-frequency tidal variations (Figures S1 and S2).

2.2. Fjord & Iceberg Measurements

The above-water iceberg digital elevation model (DEM) was constructed using structure from motion (SfM) methods in Agisoft Metashape software, converting drone imagery (DJI Phantom 4+) to a dense point cloud at ~5 cm resolution (4.1–5.7 cm), and a mesh at ~13 cm (8.7–18.1 cm; RMSE 12.4–18.7 cm). Post-processing methods were in concert with the methods of A. Crawford, Crocker, et al. (2018), using updated software. The surface DEM was then used to predict the total iceberg volume (henceforth "projected iceberg volume") using an ice density of 917 kg/m^3 and in situ average ocean properties collected from 13 conductivity, temperature, depth (CTD) profiles (Sea-Bird 25 plus CTD sensor) near the instrumented icebergs (Figure 1).

The subsurface iceberg DEM was constructed using multibeam sonar (Reason T50-P) mounted off the ship's side, which scans the depth of the iceberg to within 20 m of the water surface. However, gaps in point clouds resulted from wider portions of the iceberg impeding line of sight to the iceberg bottom, and smaller icebergs floating between the ship and the target iceberg limiting the field of view. We corrected for iceberg motion during surveying by using the geodetic GPS positions (*lat-lon*), which were comparable to an alternative method proposed by Shah et al. (2019) (see Supporting Information for expanded methods, Text S1). To construct a full-iceberg mesh (henceforth "reconstructed iceberg"), we applied a Poisson reconstruction (Kazhdan & Hoppe, 2013) to correct for gaps in subsurface data, though this method does not account for surface roughness and therefore provides a conservative measurement of the total surface area. Two of the four multibeam surveys were not complete circumnavigations due to large adjacent icebergs (scans A_1 and B_2); therefore, we only use the full-iceberg geometries from scans A_2 and B_1 to calculate iceberg surface area and subsequent melt rates.

3. Results

3.1. Iceberg Movement & Hydrology

The two icebergs transited 35 and 56 km (along-track) progressing 7 and 27 km down-fjord (Icebergs A and B, respectively; Figure 1 and Figure S3) during the 9-day study period. They incurred several short-duration direction changes, following similar fjord circulation patterns inferred from iceberg "drifters" in 2012 (Sutherland, Roth, et al., 2014). The deeper-keeled Iceberg A (~375 m) moved slower than Iceberg B (~255 m), with an average speed of 0.05 m/s (vs. 0.07 m/s, Iceberg B) and a peak speed of 0.17 m/s (vs. 0.23 m/s, Iceberg B; Figure S4). The slower speed of Iceberg A could result from more contact with Atlantic-origin water (AW; below ~150 m), which generally travels up-fjord (e.g., Straneo et al., 2011), as opposed to Polar Water (PW; >150 m) traveling down-fjord. A shift in salinity and temperature profiles was observed over the survey time and show a thinning of the PW layer (10–150 m to 10–70 m) between days 198–200, and a warming of the AW below 250 m depth over the same time period (Figure 2). Similar shifts in the PW layer have been previously observed in Sermilik Fjord (Jackson et al., 2014) and result from velocity pulses originating on the shelf adjacent to Sermilik Fjord.

3.2. Iceberg Geometry & Melt Rates

Using the reconstructed icebergs, we found the total surface area to be $1.23 \times 10^6 m^2$ and $8.52 \times 10^5 m^2$ for Icebergs A and B, and the total volume to be $5.88 \times 10^7 m^3$ and $3.47 \times 10^7 m^3$, respectively (Table 1). The reconstructed iceberg volumes are comparable to within ±10% of the projected iceberg volumes, and we attribute

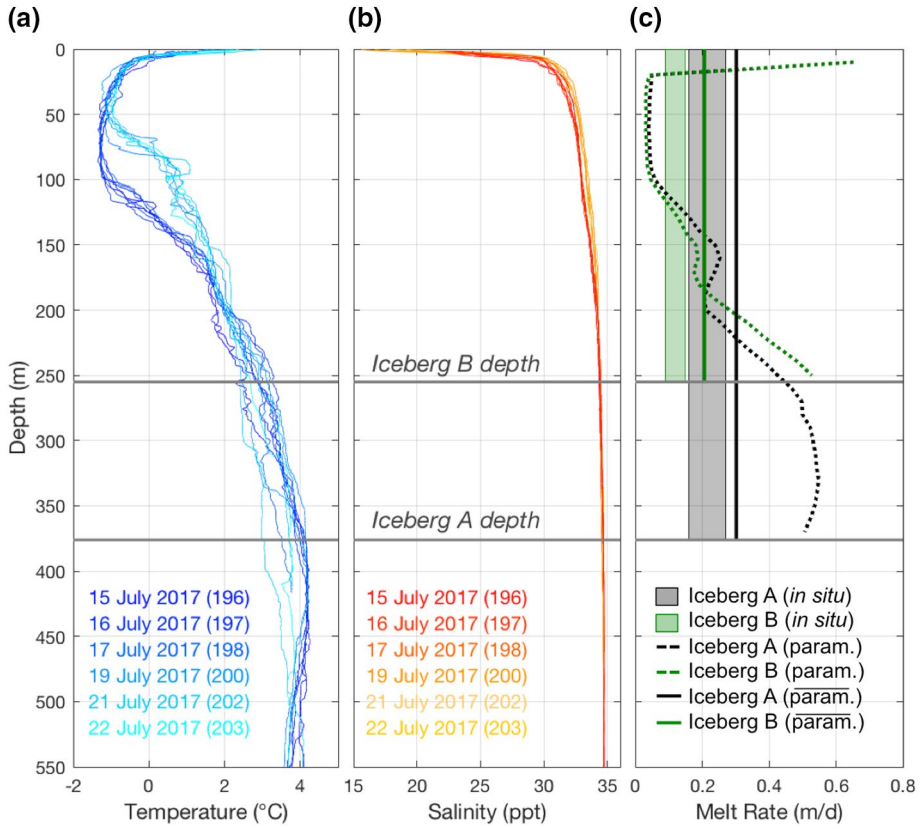

Figure 2. Temperature (a) and salinity (b) profiles collected from 13 conductivity, temperature, depth (CTD) casts adjacent to Icebergs A and B in Sermilik Fjord between July 16 and 21, 2017. Calculated melt rates with depth (c, dotted line) and depth-average melt rate (c, solid lines) are based upon melt parameterizations (e.g., Moon et al., 2018). The range of melt rates measured through in situ methods is shown by the width of the transparent green and black boxes (c).

a majority of this disparity to unknown bottom geometry; however, differences in ice density could also contribute. We found the surface length to keel depth ratio to be ~2:1, falling within the range identified in several prior multibeam studies (Barker et al., 1999), and the surface footprint (at waterline) to total volume relationship ($\text{Volume} = 6 \times \text{Area}^{x}$) to be $x = 1.31 \pm 0.01$, comparable to the findings of Sulak et al. (2017). The similarity of our measurements to prior studies suggests that even without data from the iceberg bottom, the methods presented here still capture the maximum depth and total volume.

To calculate overall melt rate, we use the surface lowering rate in combination with the projected iceberg volume to first find total volume loss, then remove the volume of mechanical ice loss (calving; calculated by differencing surface DEMs, Figure S5) to isolate volume loss due to melting. Lastly, we divide the remaining volume loss by the reconstructed surface area to calculate melt rate. After accounting for environmental variables (Figures S1 and S2), the average lowering rate for the two GPS units on Iceberg A is 9.42 ± 0.09 cm/d and 11.40 ± 0.10 cm/d, and 5.18 ± 0.12 cm/d and 6.62 ± 0.13 cm/d for the units on Iceberg B (Figure 4). Differences in surface lowering rates between GPS units on the same iceberg result from slight tilting of the iceberg surface as it melts (Figure S6).

The total volume loss for Icebergs A and B is 1.99×10^5 and 8.59×10^4 m^3/d (Table 1), with <4% of the total volume change due to calving (Figure S5). We find an overall melt rate of 0.16 and 0.10 m/d for Icebergs A and B over the 9-days instrumentation period. We also calculated melt rates based on differences in drone surveys (6 days apart), finding volume loss rates of 3.37×10^5 and 1.27×10^5 m^3/d, and melt rates of 0.27 m/d and 0.15 m/d for Icebergs A and B (Table 1, Figure S5). In isolating the corresponding 6-day period in the GPS record, we find volume loss rates of 2.18×10^5 and 7.84×10^4 m^3/d for Icebergs A and B, and melt rates of 0.18 and 0.09 m/d (Table 1).

Table 1
Iceberg Dimensions, Volumes, and Melt Rates, Calculated using a Combination of Drone Imagery, and Multibeam Sonar

	Iceberg:	A_1	A_2	B_1	B_2	A	B
2	SA_{above} ($\times 10^5$ m^2)	2.59	3.14	1.91	1.87	–	–
3	Meshed SA_{total} ($\times 10^5$ m^2)	–	12.3	8.52	–	–	–
4	V_{above} ($\times 10^6$ m^3)	6.97	6.76	3.38	3.30	–	–
5	Projected V_{total} ($\times 10^7$ m^3)	6.52	6.34	3.17	3.10	–	–
6	Meshed V_{total} ($\times 10^7$ m^3)	–	5.88	3.47	–	–	–
7	Surface length (m)	733	729	518	515	–	–
8	Keel depth (m)	386	375	255	251	–	–
9	height (avg) (m)	35.1	34.1	22.6	22.5	–	–
10	height (max) (m)	56.8	55.9	51.8	51.9	–	–
11	Atm pressure (hPa)	998.3	1,006.8	998.5	1,006.5	–	–
12	Total Vol. Loss (GPS,$\times 10^5$ m^3/d) 9 days	–	–	–	–	1.99	0.86
13	Total Vol. Loss (GPS,$\times 10^5$ m^3/d) 6 days	–	–	–	–	2.18	0.78
14	Total Vol. Loss (drone,$\times 10^5$ m^3/d) 6 days	–	–	–	–	3.37	1.27
15	Mechanical Loss (drone,$\times 10^3$ m^3/d) 6 days	–	–	–	–	6.36	5.04
16	Melt Rate (GPS, m/d) 9 days	–	–	–	–	0.16	0.10
17	Melt Rate (GPS, m/d) 6 days	–	–	–	–	0.18	0.09
18	Melt Rate (drone, m/d) 6 days	–	–	–	–	0.27	0.15

Notes. Iceberg dimensions are calculated from drone imagery (rows 2, 4, 5, 7, 9, 10), multibeam sonar (row 8), and a combination of drone and multibeam sonar (rows 3, 6) for Iceberg A (columns 3, 6) and Iceberg B (columns 5, 6). Atmospheric pressure (row 11) is used to correct freeboard height in the projected iceberg volume calculation (row 5). Volume loss rates for Icebergs A (column 7) and B (column 8) are calculated using GPS lowering (row 12 and 13) and drone volume measurements (rows 14 and 15). Measurements of volume loss rate and melt rate have been partitioned based upon the instrumental period (9 days) and the time between drone surveys (6 days).

The melt rate for Icebergs A and B over the 9-day period showed temporal variability, we therefore isolated average melt rates of 0.18 m/d (day 198.9–201.75) and 0.10 m/d (day 201.75–203.5) for Iceberg A, and 0.06 m/d (mass gain, day 198.9–200), 0.15 m/d (day 200–202.5), and 0.09 m/d (day 202.25–203.5) for Iceberg B based upon slope breaks. The increase in melt rates around day 200, for both Icebergs A and B, coincides with changes in fjord hydrography, specifically a warming of the PW layer and a slight cooling of the AW layer. The apparent mass gain in Iceberg B is likely an artifact due to tipping, as identified in differenced surface DEMs (Figure S6; tilting uncertainty calculations in Supporting Information, Text S1).

4. Discussion

4.1. Iceberg Melt Rates

We propose that the difference in overall melt rate between Icebergs A and B results from differences in keel depth, and therefore differences in the proportion of each iceberg in contact with variable water layers. Sermilik Fjord contains multiple temperature and salinity changes over its 900 m depth (Straneo et al., 2016; Sutherland, Straneo, & Pickart, 2014), and much more of Iceberg A exists in the warmer water below the AW/PW interface (Figure 2). This layering could explain the higher average melt rate observed for Iceberg A. However, we also observe variable melt rates within the 9-day survey period, congruent with changes in the AW/PW interface depth, potentially resulting from short-duration changes in fjord circulation.

Changes in the AW/PW interface depth are accompanied by increased current speeds (Figure S4). This pulse mirrors findings in Jackson et al. (2014), where the vertical gradient of the horizontal velocity also moves up and down. Thus, over the course of the survey period, the PW layer thinned, bringing warmer water to shallower depths, while at the same time increasing relative water motion and a coincident small cooling below 275 m (Figure 3). The deeper-keeled Iceberg A would have experienced both the warming

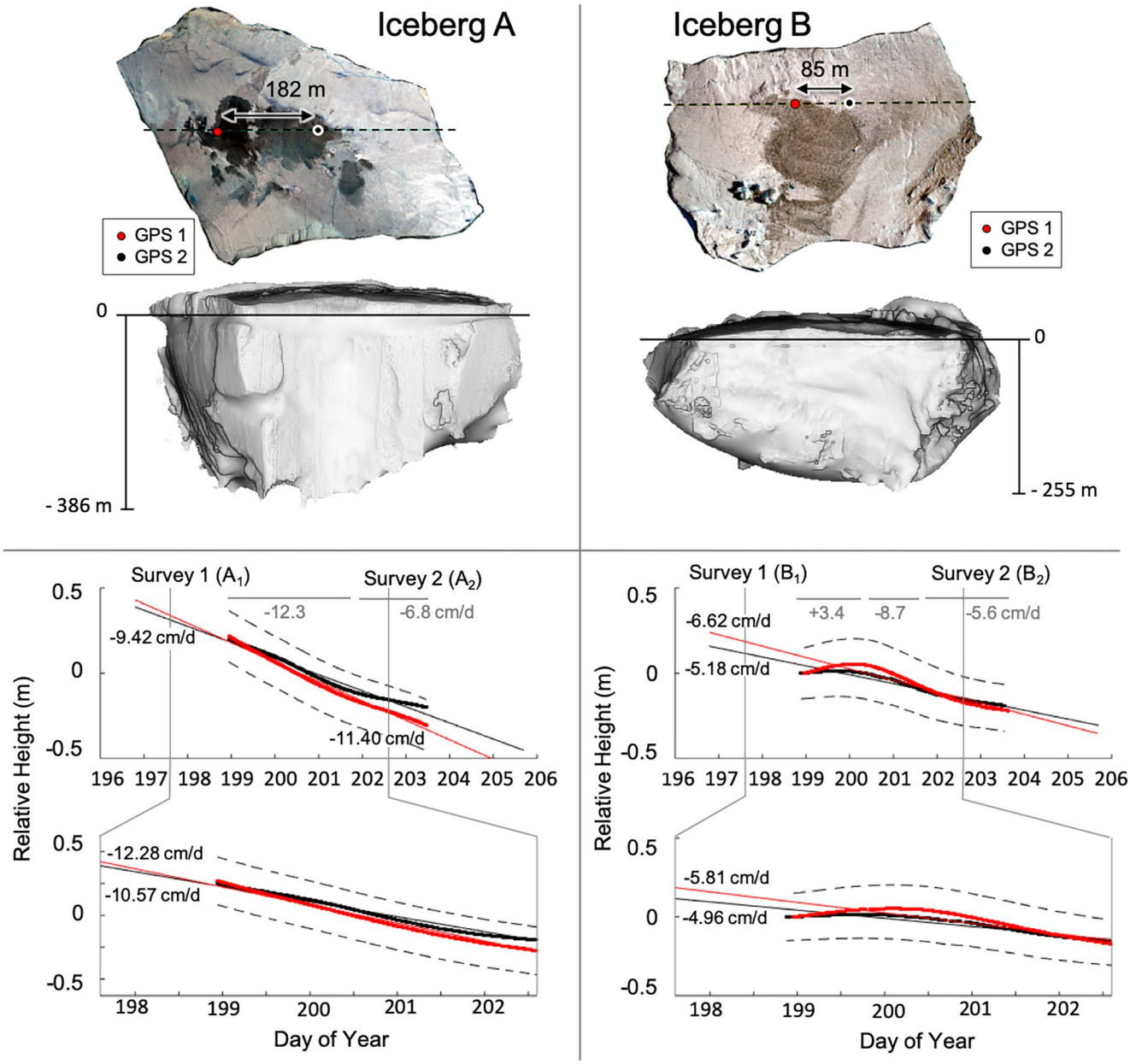

Figure 3. Full-iceberg geometries constructed from drone and multibeam surveys (top) with the location of each geodetic GPS noted (red and black circles). Iceberg height measurements (with tilting uncertainties, dashed, see Supporting Information Text S1) after accounting for environmental variables and applying a 40-h Hanning filter (bottom) for both the 9 and 6-day survey periods. Linear trend lines show the surface lowering rates (values noted) for each GPS unit and gray horizontal lines show the average surface lowering rates for specific periods.

and cooling waters and less effect from the increased currents given that its keel depth spans across the oppositely flowing layers, whereas Iceberg B would only have experienced warmer waters, thereby increasing the depth-averaged melt rate. The difference in depth-averaged melt rate of Icebergs A and B implies that both depth-dependent hydrography changes and depth-dependent horizontal velocities are impacting the overall melt rate, and therefore a depth-dependent melt rate must also exist.

The differing melt rate data suggest that a key second control on iceberg melt rate is water velocity relative to iceberg movement. Over the 9-days survey period, the icebergs changed flow direction (inflow to outflow) in concert with changes in the AW/PW interface depth. The shallower-keeled Iceberg B shows a strong trend of increasing melt rates with increased velocity (Figure 4). Prior to the flow reversal and thinning of the

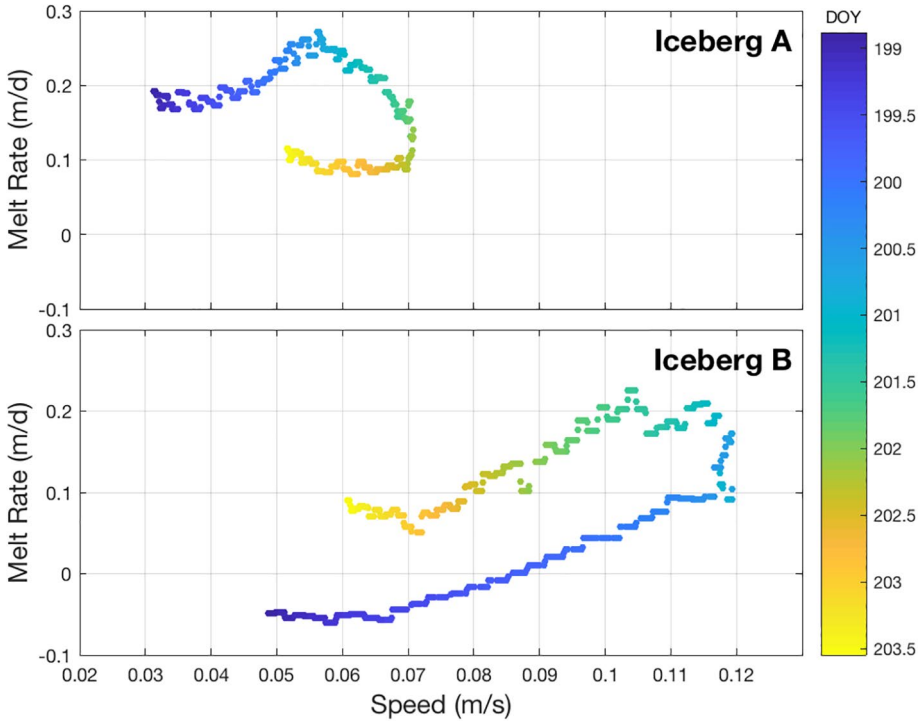

Figure 4. Melt rate versus iceberg speed for Icebergs A (top) and B (bottom), with color indicating day of year. Higher melt rates correspond with higher volume loss rates, and negative rates indicate an increase in surface elevation, likely due to iceberg tipping (Figure S6).

PW layer, Iceberg B shows lower overall melt rates, which later increased for the same velocities as the AW/PW interface shoaled (Figure 4). Conversely, Iceberg A did not show any strong relationship between melt rates and iceberg velocity. We hypothesize this is due to the dual control of temperature and relative velocity on iceberg melt rate: Iceberg A's deeper keel leads to diminished depth-averaged velocities with a greater portion of its subsurface area in the warmer AW layer, implying higher relative velocities and a higher mean temperature. Iceberg B doubled its speed during the inflow event as it resides more squarely in the upper PW layer, yet as the PW layer thinned, the melt rates stayed high even as the water velocities decreased again (hysteresis shown in Figure 4).

4.2. Comparison to Prior Methods

The depth-averaged iceberg melt rates presented here (0.09–0.27 m/d) are comparable but smaller than those calculated for deep-keeled icebergs in recent remote sensing studies for Sermilik Fjord (e.g., Enderlin et al., 2016). We attribute this to two fundamental differences: (1) the subsurface geometry used in calculations, and (2) the spatial resolution of measurements. Problematically, the use of end-member geometries (cone and cylinder) greatly underestimates iceberg surface area (22%–43%; see Supporting Information, Text S1) and therefore over-estimates melt rates given the same mass loss rates, also hindering the ability to be compared to melt rates using different subsurface geometries. Spatial resolution in remote sensing studies can be as high as 0.55 m with DEM resolution as high as ~2 m ± 3 m, however, edge detection remains a challenge due to mixed pixels, and often necessitates exclusion of these side areas (Enderlin et al., 2016, 2018; Enderlin & Hamilton, 2014). While removal reduces errors, it also excludes a key potential area of volume loss through calving, impacting subsequent volume loss calculations. In order to, better constrain iceberg loss and up-scale to include more iceberg variability, high temporal and spatial in situ studies, such as this study, should be combined with remote sensing efforts. Additionally, the reliance of subsurface geometry, and therefore survey method, to establish overall melt rate is a limitation in iceberg studies and necessitates the presentation of mass loss rates (m^3/d) in addition to melt rates to facilitate inter-study comparison as methodology and technology develops.

We also compare the depth-averaged melt rates to a theoretical melt model using in situ measurements for standard melt parameterizations (see Supporting Information, Text S1). We found the average modeled melt rates were higher than our measurements at 0.30 m/d and 0.21 m/d (±30%) for Icebergs A and B, respectively (Figure 3). However, calculated melt rates with depth, which include depth-dependent dominant erosion processes, found a melt rate range of 0.05–0.65 m/d. This model demonstrates how two icebergs in the same fjord can have different depth-averaged melt rates due to the overlap of their individual subsurface geometry with stratification and velocity shear in the water column, thereby supporting observations of different melt rates for Icebergs A and B.

5. Conclusion

During July 2017, we collected simultaneous glaciological and oceanographic in situ measurements of iceberg deterioration and full geometry of two large icebergs in Sermilik Fjord, southeast Greenland. We used a combination of coincident on-iceberg geodetic GPS to measure surface lowering, and ship-based drone and multibeam sonar data to construct full-iceberg geometries. We used individual iceberg geometry to calculate iceberg melt rates first based upon GPS surface lowering, and then differences in repeat surface DEMs. We found melt rates lower than those from previous studies in southeast Greenland, likely due to using individual geometries in melt rate calculations. We calculated that end-member geometries underestimate subsurface area by at least 22%–43%, leading to an overestimate in melt rate for the same volume loss. These results necessitate the development of representative geometries to use in future remote sensing and modeling studies and the inclusion of volume loss rates (m^3/d) to minimize method-dependent results.

This synthesis of iceberg geometry and GPS data to constrain the in situ melt measurements is among the first of its kind. Using the methods of calculating mass loss, we found variable average melt rates for both icebergs. While the icebergs were large (>500 m length) and were subjected to near identical environmental forcing, the deeper keeled iceberg experienced a higher average melt rate in all calculations (GPS lowering, drone differencing, model parameterization), providing strong support for depth-dependent melt rates, variable on the time scale of days. These results support the development of depth-dependent iceberg melt rates given depth-dependent hydrography and water velocities.

Data Availability Statement

Processed SfM drone pointclouds, raw GPS data, multibeam pointclouds (doi: 10.18739/A2QF8JK6B), and CTD casts (doi: 10.18739/A2NG4GS8C) are uploaded to the Arctic Data Center.

Acknowledgments
This work was supported by NSF OPP grant 1552232. We would like to thank Michael Kazhdan for his help in full-iceberg geometry reconstructions, AirGreenland Pilot Bent Reiss for helicopter support, CPS for logistic support, the MV Adolph Jensen captain and crew, and Fiammetta Straneo, William Ostrom, Dustin Carroll, Jamie Holte, Isabella LeBras, and Elizabeth Brasseale for assisting in data collection, and Eryl Derome, Chris Eckert, Jason SooHoo, and Ken Wilson for GPS engineering. We also thank Till Wagner and Gordy Stephenson for their helpful reviews. There are no financial conflicts of interests for any author.

References

Allan, D., & Allan, R. P. (2019). Seasonal changes in the North Atlantic cold anomaly: The influence of cold surface waters from coastal Greenland and warming trends associated with variations in subarctic Sea ice cover. *Journal of Geophysical Research: Oceans*, *124*(12), 9040–9052. https://doi.org/10.1029/2019jc015379

Bamber, J., van den Broeke, M., Ettema, J., Lenaerts, J., & Rignot, E. (2012). Recent large increases in freshwater fluxes from Greenland into the North Atlantic. *Geophysical Research Letters*, *39*(L19501), 4. https://doi.org/10.1029/2012GL052552

Barker, A., Sayed, M., & Carrieres, T. (2004). Determination of iceberg draft, mass and cross-sectional areas. In *The Fourteenth International Offshore Polar Engineering Conference* (pp. 899–904). Toulon: International Society of Offshore and Polar Engineers.

Barker, A., Skabova, I., & Timco, G. (1999). In C. H. Centre (Ed.), *Iceberg visualization database*. Ottawa, Canada: National Research Council Canada, Canadian Hydraulics Centre.

Crawford, A., Crocker, G., Mueller, D., Desjardins, L. U. C., Saper, R. O. N., & Carrieres, T. O. M. (2018). The canadian ice island drift, deterioration and detection (CI2D3) database. *Journal of Glaciology*, *64*(245), 517–521. https://doi.org/10.1017/jog.2018.36

Crawford, A. J., Mueller, D., & Joyal, G. (2018). Surveying drifting icebergs and ice islands: Deterioration detection and mass estimation with aerial photogrammetry and laser scanning. *Remote Sensing*, *10*(4), 575. https://doi.org/10.3390/rs10040575

Dukhovskoy, D. S., Yashayaev, I., Proshutinsky, A., Bamber, J. L., Bashmachnikov, I. L., Chassignet, E. P., et al. (2019). Role of Greenland freshwater anomaly in the recent freshening of the subpolar North Atlantic. *Journal of Geophysical Research: Oceans*. *124*(5), 3333–3360. https://doi.org/10.1029/2018jc014686

El-Tahan, M., Venkatesh, S., & El-Tahan, H. (1987). Validation and quantitative assessment of the deterioration mechanisms of Arctic icebergs. *Journal of Offshore Mechanics and Arctic Engineering*, *109*(1), 102–108. https://doi.org/10.1115/1.3256983

Enderlin, E. M., Carrigan, C. J., Kochtitzky, W. H., Cuadros, A., Moon, T., & Hamilton, G. S. (2018). Greenland iceberg melt variability from high-resolution satellite observations. *The Cryosphere*, *12*(2), 565–575. https://doi.org/10.5194/tc-12-565-2018

Enderlin, E. M., & Hamilton, G. S. (2014). Estimates of iceberg submarine melting from high-resolution digital elevation models: Application to Sermilik Fjord, East Greenland. *Journal of Glaciology*, *60*(224), 1084–1092. https://doi.org/10.3189/2014JoG14J085

Enderlin, E. M., Hamilton, G. S., Straneo, F., & Sutherland, D. A. (2016). Iceberg meltwater fluxes dominate the freshwater budget in Greenland's iceberg-congested glacial fjords. *Geophysical Research Letters*, *43*(21), 11287–11294. https://doi.org/10.1002/2016gl070718

FitzMaurice, A., Cenedese, C., & Straneo, F. (2018). A laboratory study of iceberg side melting in vertically sheared flows. *Journal of Physical Oceanography*, *48*(6), 1367–1373. https://doi.org/10.1175/jpo-d-17-0185.1

Gagnon, R. E., & Wang, J. (2012). Numerical simulations of a tanker collision with a bergy bit incorporating hydrodynamics, a validated ice model and damage to the vessel. *Cold Regions Science and Technology*, *81*, 26–35. https://doi.org/10.1016/j.coldregions.2012.04.006

Good, P., Bamber, J., Halladay, K., Harper, A. B., Jackson, L. C., Kay, G., et al. (2018). Recent progress in understanding climate thresholds. *Progress in Physical Geography: Earth and Environment*, *42*(1), 24–60. https://doi.org/10.1177/0309133317751843

Jackson, R. H., Straneo, F., & Sutherland, D. A. (2014). Externally forced fluctuations in ocean temperature at Greenland glaciers in non-summer months. *Nature Geoscience*, *7*(7), 503–508. https://doi.org/10.1038/ngeo2186

Josberger, E. G. (1978). A laboratory and field study of iceberg deterioration. In A. A. Husseiny (Ed.), *Iceberg utilization for fresh water production, weather modification and other applications* (pp. 245–264). Ames, IA: Pergamon Press.

Kazhdan, M. M., & Hoppe, H. (2013). Screened poison surface reconstruction. *ACM Transactions on Graphics*, *32*, 29.

Marsh, R., Desbruyeres, D., Bamber, J. L., de Cuevas, B. A., Coward, A. C., & Aksenov, Y. (2010), Short-term impacts of enhanced Greenland freshwater fluxes in an eddy-permitting ocean model, *Ocean Science*, *6*(3), 749–760. https://doi.org/10.5194/Os-6-749-2010

McKenna, R. F. (2005). Refinement of iceberg shape characterization for risk to Grand Banks installations, edited. In *Canadian Hydraulics Center* (p. 84). National Research Council Canada. https://doi.org/10.4224/12328384

Moon, T., Sutherland, D. A., Carroll, D., Felikson, D., Kehrl, L., & Straneo, F. (2018). Subsurface iceberg melt key to Greenland fjord freshwater budget. *Nature Geoscience*, *11*(1), 49–54. https://doi.org/10.1038/s41561-017-0018-z

Mouginot, J., Rignot, E., Bjork, A. A., van den Broeke, M., Millan, R., Morlighem, M., et al. (2019). Forty-six years of Greenland ice sheet mass balance from 1972 to 2018. *Proceedings of the National Academy of Sciences of the United States of America*, *116*(19), 9239–9244. https://doi.org/10.1073/pnas.1904242116

Shah, V., Schild, K., Lindeman, M., Duncan, D., Sutherland, D., Cenedese, C., et al. (2019). Multi-sensor mapping for low contrast, quasi-dynamic, large objects. *IEEE Robotics and Automation Letters*, *5*(2), 470–476.

Straneo, F., Curry, R. G., Sutherland, D. A., Hamilton, G. S., Cenedese, C., Vage, K., & Stearns, L. A. (2011). Impact of fjord dynamics and glacial runoff on the circulation near Helheim Glacier. *Nature Geoscience*, *4*(5), 322–327. https://doi.org/10.1038/ngeo1109

Straneo, F., Hamilton, G. S., Stearns, L. A., & Sutherland, D. A. (2016). Connecting the Greenland Ice Sheet and the Ocean: A case study of Helheim Glacier and Sermilik Fjord. *Oceanography*, *29*(4), 34–45. https://doi.org/10.5670/oceanog.2016.97

Sulak, D. J., Sutherland, D. A., Enderlin, E. M., Stearns, L. A., & Hamilton, G. S. (2017). Iceberg properties and distributions in three Greenlandic fjords using satellite imagery. *Annals of Glaciology*, *58*(74), 92–106. https://doi.org/10.1017/aog.2017.5

Sutherland, D. A., Roth, G. E., Hamilton, G. S., Mernild, S. H., Stearns, L. A., & Straneo, F. (2014). Quantifying flow regimes in a Greenland glacial fjord using iceberg drifters. *Geophysical Research Letters*, *41*(23), 8411–8420. https://doi.org/10.1002/2014GL062256

Sutherland, D. A., Straneo, F., & Pickart, R. S. (2014). Characteristics and dynamics of two major Greenland glacial fjords. *Journal of Geophysical Research: Oceans*, *119*(6), 3767–3791. https://doi.org/10.1002/2013jc009786

Venkatesh, S., El-Tahan, H., & Mitten, P. T. (1985). An Arctic iceberg deterioration field study and model simulations. *Annals of Glaciology*, *6*, 195–199.

Wagner, T. J. W., Stern, A. A., Dell, R. W., & Eisenman, I. (2017). On the representation of capsizing in iceberg models. *Ocean Modelling*, *117*, 88–96. https://doi.org/10.1016/j.ocemod.2017.07.003

Weeks, W. F., & Campbell, W. J. (1973). Icebergs as a fresh-water source: An appraisal. *Journal of Glaciology*, *12*(65), 207–233. https://doi.org/10.3198/1973JoG12-65-207-233

White, F. M., Spaulding, M. L., & Gominho, L. (1980). *Theoretical estimates of the various mechanisms involved in iceberg deterioration in the open ocean environment*. U. S. C. Guard.

Yang, Q., Dixon, T. H., Myers, P. G., Bonin, J., Chambers, D., van den Broeke, M. R., et al. (2016). Recent increases in Arctic freshwater flux affects Labrador Sea convection and Atlantic overturning circulation. *Nature Communications*, *7*, 10525. https://doi.org/10.1038/ncomms10525